Research Square

Preprints are preliminary reports that have not undergone peer review.
They should not be considered conclusive, used to inform clinical practice,
or referenced by the media as validated information.

In vivo characterization of electrodes for selective stimulation of neurovascular bundles during robot-assisted radical prostatectomy

Janez Rozman

jnzrzmn6@gmail.com

ITIS d. o. o. Ljubljana

Jure Bizjak

University Medical Centre Ljubljana

Tomaž Smrkolj

University Medical Centre Ljubljana

Samo Ribarič

Faculty of Medicine, University of Ljubljana

Simon Hawlina

University Medical Centre Ljubljana

Research Article

Keywords: neurovascular bundle, platinum, stimulating electrode, interface, voltage response, EMG

Posted Date: April 28th, 2026

DOI: https://doi.org/10.21203/rs.3.rs-9440557/v1

License: This work is licensed under a Creative Commons Attribution 4.0 International License.
Read Full License

Additional Declarations: No competing interests reported.

Abstract

The electrical and electrophysiological performance of platinum electrodes within the probe for bipolar selective stimulation of neurovascular bundles (NVB)s during robot-assisted radical prostatectomy was investigated. Quasi-trapezoidal pulse trains (5 min) were delivered to isolated NVBs in 5 patients. The electrical performance of the electrodes was studied by determining the polarization across the electrode–NVB tissue interface using voltage transients. Cavernous EMG (CC-EMG), axial rigidity and computing CC-EMG features were measured in the frequency domain. The most negative E_{mc} and most positive E_{ma} potentials across the electrode–NVB tissue interface reached − 11.49 V and 11.52 V, respectively; the cathodal (σQ_c) and anodal (σQ_a) charge densities were 0.963 μA s/mm^2 and 0.435 μA s/mm^2, respectively. They exceeded tissue injury limits for a short time, but tissue injury did not occur. Impedance $|Z|$ decreased faster with frequency in vitro (50 Hz, 170 Ω) than in vivo (1500 Ω). The median frequencies of the amplitude and power were: CC-EMGr, 26.7 Hz and 50 Hz; CC-EMGl, 28.33 Hz and 43.58 Hz. Both were contaminated with the stimuli and facility mains. Any influence of τ_{exp} preset in the stimuli on electrophysiological performance could not be identified. An increase in penile axial rigidity was not observed in any patient.

Introduction

Radical prostatectomy is the surgical treatment for patients with prostate cancer [1–3]. However, it is difficult to remove the gland without affecting prostate neurovascular bundles (NVB)s that innervate the corpora cavernosa (CC) [4–6].

Efferent innervation of the penis comes from parasympathetic, sympathetic and somatic sources. Somatosensory afferents, however, course from the penis to central sites [7, 8]. NVBs are composed of thin, wiry post-ganglionic parasympathetic nerves expanding from the pelvic hypogastric plexus. They contain delicate bundles of cavernous nerve (CN) fibres, prostatic branches of the inferior vesical artery, prostatic veins, collagen fibres and adipose tissue, all surrounded by connective tissue. They travel posterolaterally to the prostate, eventually reaching the spongy erectile tissues of the CC [9]. Parasympathetic CN fibres that arise from the prostatic plexus innervate the helicine arteries of the erectile tissue in the cavernous spaces. They mediate vasodilation and stimulate the erection of the penis. They are extremely susceptible to stretch. Rodrigues et al. [10] assumed that numerous nerve fibres are located in the anterior and anterolateral positions and that CNs are probably formed by the posterior nerve fibres located at a safer distance from the prostate.

Despite recent advances in surgical techniques, erectile dysfunction still occurs as a consequence of injury caused during radical prostatectomy, mainly to the CNs and less to the arteries within the NVB. A surgical technique called nerve-sparing prostatectomy was developed to preserve the NVBs [1, 2]. When appropriately accomplished during robot-assisted radical prostatectomy (RARP), nerve sparing largely improves recovery of erectile function (EF). Robotic assistance offers excellent visualization of the NVBs and high surgical precision [1–3]. However, despite advancements in NVB preservation, potency rates

have remained unsatisfactory. Tode et al. [11] showed that regeneration after injury is limited because afferent axons regenerate into the peripheral nerve stump. Thus, even when spared, the recovery of EF may take months after the procedure [3, 10]. Therefore, the focus is on how to improve RARP techniques to preserve the functionality of the NVBs. Intraoperative nerve monitoring was introduced as a technique to assist the surgeon in minimizing the risk of harm to the NVBs. The technique was based on investigations on the distribution of CN fibres around the prostate using nerve stimulation during radical prostatectomy [12].

In recent decades, the concepts for electrical nerve stimulation involved non-fibre-selective stimulation, which in turn frequently causes undesirable effects. Accordingly, various models of selective nerve fibre stimulation and electrodes that selectively stimulate certain features have been developed [13, 14].

Peripheral nerve fibres are classified into 4 subclasses according to their diameter, conduction velocity, and extent of myelination [15, 16]. One subclass is a large group of unmyelinated slowly conducting C-fibres with axon diameters from 0.2 μm to 1.2 μm and up to 3 μm in some cases. They are widely distributed in hairy and glabrous skin, transmitting cutaneous and visceral peripheral signals to the central nervous system. C-fibres are also present in the glabrous skin of the glans penis. They play a crucial role in the nervous transmission of peripheral sexual stimuli to higher cortical sexual arousal areas [16, 17]. Generally, unmyelinated C-fibres that have higher stimulation thresholds (between 1 and 3 mA) are activated less reliably than myelinated ones (about 0.15 mA) and stay activated for higher currents. The exact threshold depends on the stimulation frequency, pulse duration and electrode placement. C-fibres typically require higher stimulation intensities or longer duration than Aβ- and Aδ-fibres [15, 16]. Therefore, the intensity, frequency and pattern of electrical stimuli play a critical role in determining which fibre types are activated. Other fibre types, such as thinly myelinated Aδ-fibres, can also be activated at certain frequencies; 5 Hz is often cited for C-fibre activation, but the optimal range for C-fibre stimulation is broader. Frequencies between 20 and 50 Hz have been identified as the blocking frequency for C-fibre afferents [18].

In CN stimulation, a frequency range of 10–20 Hz, pulse duration 0.5–1 ms, stimulation duration 30–60 s and voltage 2.5–8 V are commonly used to induce erectile responses [19]. NVBs require high charge densities for stimulation due to a high content of non-myelinated nerve C-fibres [20, 21]. This may result in a high energy transfer and the occurrence of reversible and potentially irreversible chemical reactions.

The use of current, biphasic stimulating pulses in neural tissue stimulation, with cathodal and anodal phases of equal shape and charge per phase, is a common practice [22, 23]. Charge delivery has been shown to be highly influenced by the electrode–NVB interface, where transduction of electrons in the metallic electrode to ions in the tissue occurs [24, 25]. Accordingly, impedance $|Z|$ that occurs at the electrode–NVB interface is crucially affected by the electrode geometry. The efficiency of neural excitation, however, is highly dependent on the current density on the electrode surface and the spatial distribution of the electric field generated in the tissue [26].

Although efforts have been made to find optimum positions at the NVB, little work has been done to test the efficiency of NVB stimulation using analytically driven configurations of the electrodes and stimulus waveforms. Warman et al. [27] showed that nerve fibre excitation could be predicted using the driving function of a neuron, which is proportional to the second spatial derivative of the extracellular potential and thus, the spatial derivative of the current density in the tissue. Accordingly, an electrode with greater roughness would increase the efficiency of the nerve fibre stimulation [26, 27].

Every material appropriate for the production of electrodes has a charge that delimits reversibility and irreversibility of the electrochemical processes at the interface. Pure platinum is frequently used because it can inject charge by both double-layer charging and Faradaic processes [28, 29]. However, they can be either reversible or irreversible. It was shown that all irreversible electrochemical processes are harmful. The platinum charge injection limits within which the electrolysis of water is avoided in chronic stimulation with biphasic cathode first pulses were determined to be between 50 and 150 μC cm^{-2} (geometric area) [29–31]. Platinum as a stimulating electrode material has the advantage of decreasing |Z| with increasing frequency. In vitro electrochemical techniques such as cyclic voltammetry, |Z| and voltage transient (SVT) measurements can be used to characterize an electrode for nerve tissue stimulation [32, 33]. Their results enable the selection and design of the electrode material, and selection of stimulation pulse waveform and parameters for efficient and safe nerve tissue stimulation [24, 34].

SVTs are frequently used to estimate the charge injection limit Q_{inj}, which defines the charge that can be injected by the electrode in a current stimulation pulse using only reversible processes. SVTs determine both negative (E_{mc}) and positive (E_{ma}) potential extremes across the electrode–electrolyte interface. These potential extremes are then compared with the established maximum potentials beyond which it is considered unsafe to polarize the electrode (typically the potential window of water electrolysis). In most in vivo testing, however, the electrode is placed onto or into the neural tissue to develop the electrode–NVB interface [32, 33].

Corpus cavernous EMG (CC-EMG) is a measure of the electrical activity of the smooth corpus cavernosum muscle (CCM), which is a prerequisite for erection. According to Wagner et al. [35], CC-EMG is the most direct electrophysiological indicator of any malfunction in the integrity circuits between the CNS and CCM related to EF. Klotz and Herschorn [36] described how to successfully capture CC-EMG during prostatectomy. Some authors claimed that CC-EMG reflects the summation of the membrane current of a group of CCM muscle cells and is the source of the electrical activity that may be measured [37–40]. Much later, Vírseda-Chamorro et al. [41] declared that CC-EMG of the erectile tissue recorded during erection could be used as a diagnostic technique in patients with erectile dysfunction. In addition, Leddy et al. [42] have identified the origin of the low-frequency CC-EMG complexes in volunteers with normal EF using penile surface electrodes. They concluded that the CCM tissue was the origin of the CC-EMG complex and not the penile skin or surrounding tissue.

Recently, Yildiz et al. [43] aimed to evaluate the changes in penile sensation using electrophysiological tests in patients who underwent RARP. The results showed decreased penile sensation due to CN

damage and a possible dorsal penile nerve injury. However, the CC-EMG generating source is still not clearly known [44, 45]. Monopolar needle electrodes and/or non-invasive surface electrodes placed on the penis could be used for CC-EMG recording. Amplification of CC-EMG and attenuation of environmental noise can be accomplished using a differential amplifier [45, 46]. However, a low-pass and high-pass filter should be used to acquire the most optimal frequency range of the CC-EMG (0.1–5 Hz), and a notch filter should be used to remove the noise from the power lines [47].

Jiang et al. [45] showed that peripheral autonomic injuries could be suspected if the amplitude and duration of CC-EMG signals diminished. Thus, careful and thorough CC-EMG monitoring during RARP may provide further information useful for preserving EF.

The present work focuses on modelling and in vivo testing of the geometry of the cathode and waveform of a stimulating pulse based on the electrochemical and neurophysiological mechanisms to provide efficient, safe and potentially selective fibre-type NVB stimulation. A concept capable of preferential activation of a population of C-fibres in an NVB to potentially effect faster, stronger and more durable erections was proposed. We tested our hypothesis that such stimulating electrodes could activate a population of nerve fibres within the NVB in a more physiological manner in vivo during RARP. The ultimate intention was to estimate the usability of the concept in further development of an intraoperative measuring procedure aimed at improving recovery of EF after prostatectomy.

Methods

Design of stimulating pulse and electrodes

The NVB is composed of myelinated Aδ-fibres, also designated as B-fibres (diameter [D] = 1–5 µm, $CV_{A\delta}$=3–15 m/s), and unmyelinated C-fibres (D = 0.5–2 µm, CV_c=0.5–2 m/s) [10, 16]. Most are C-fibres; B-fibres are in the minority. The differing properties of each individual fibre result in different action potential (AP) thresholds, refractory periods, and the duration of the APs [48, 49]. Consequently, any change in the amplitude and waveform of the CC-EMG is due to a change in the number of fibres that are firing. With increasing stimulation current i_c, however, the number of axons firing is equivalent to the sum of all those whose thresholds are met by a given input. The latency between the application of the stimulus and the onset of the CC-EMG is a function of the events during the depolarization and an autonomic signal path between the recording site and the site of the stimulation. It was assumed that the i_c, required for activation of the AP in Aδ-fibres, is significantly lower than that required for C-fibre activation [50, 51], that Aδ- and C-fibres could be activated at any site on the cathode and that the APs elicited would propagate simultaneously in both directions. According to the paradigm, the AP in the C-fibres should reach the inner edge of the circular anode (A) after i_c has exponentially decayed to a point that is inefficient at blocking their conduction [52]. It was assumed that the latest AP of the Aδ-fibres, however, arrives at the inner edge of the anode and passes away as the hyperpolarizing effect of the anode is weak. For this purpose, the time separations between the AP of Aδ- and C-fibres to reach the inner edge of an anode were calculated. The intensity of the anodal phase of the stimulus had to be

lower than the threshold of the anodal activation of the Aδ-fibres to prevent excitation due to reversed polarity on the cathode during the anodal phase. On the anode, hyperpolarization caused by inward current should be decayed exponentially to prevent any anodal break excitation when APs arrive from the cathode. Activation of fibres with different conduction velocity (CV) could therefore be achieved by changing the time constant τ_{exp} of exponential i_c decay and by adjusting the intensity of i_c. The resulting stimulus shown in Fig. 1b was a current, charge-balanced pulse composed of a quasi-trapezoidal cathodal phase with a square leading edge of intensity i_c, a plateau of the cathodal phase with the width of t_c, followed by an exponentially decaying phase with the width of t_{exp} and the time constant τ_{exp}, and ended with a wide, rectangular, anodic phase with width t_a and intensity i_a.

The electrodes for NVB stimulation were designed considering the published results of studies modelling the selective stimulation of peripheral nerves [27, 50, 52], the available structural topography of the NVBs, and the paradigm developed. The distributions of the fibre diameters and physical dimensions were taken from the literature to define the relationship between the structural topography and the physical model [7, 15, 16]. For the NVB simulation, the aforementioned quasi-trapezoidal biphasic rectangular and cathodal first current stimulating pulse pairs with a frequency of 10 Hz were intended to be delivered to the NVB via specifically designed stimulation electrodes. The quantities that were considered for the design of the stimulation pulse and stimulation electrodes are presented in Table 1.

Table 1
Quantities considered for the design of the stimulating probe

Parameter	Acronym	Value
Type of nerve fibre	NA	A_δ, C
Diameter of A_δ-fibres	$d_{A\delta}$	1–5 µm
Diameter of C-fibres	d_c	0.5–2 µm
Conduction velocity of A_δ-fibres	$CV_{A\delta}$	3–15 m/s
Conduction velocity of C-fibres	CV_c	0.5–2 m/s
Average conduction velocity of C- and A_δ-fibres	CV_{av}	8 m/s
Distance from the centre if the cathode to the circular edge	D_{ce}	3.7 mm
Average travel time of the action potential from the centre of the cathode to the anode	t_{ce}	465 µs

Manufacture of the stimulating probe

The material used to craft the stimulation electrodes with a specific shape and arrangement was chosen based on the mechanical and electrochemical characteristics [32, 33]. A spiral-shaped stimulation cathode and a ring-shaped anode were crafted from a 0.25-mm-thick cold-rolled platinum ribbon (purity, 99.99 wt %) (Zlatarna Celje d. d., Kersnikova 19, 3000 Celje, Republic of Slovenia). The first step in crafting the electrodes involved the design and computer-supported drawings of the arrangement at dimensions that matched the proposed paradigm. A file of the drawings was then transferred to the laser cutting machine to cut out an electrode arrangement from the platinum ribbon. Once cut out, the geometric surface of the cathode obtained was 27 mm^2 and that of the anode was 23 mm^2. In the third step, a piece of platinum wire was welded onto the back of each electrode using a capacitive discharge spot welder. In addition, a few additional bent pieces were welded on both electrodes as anchors within an encapsulant to prevent the electrodes from separating from the probe. Lead wires to the electrodes made of fluorinated ethylene propylene (FEP) insulated stranded wire (AS 637, Cooner Wire, Chatsworth, CA) were welded onto the 2 pieces of platinum wire.

Self-curing denture material (ProBase Cold Professional PMMA denture base material, Ivoclar, Schaan, Liechtenstein) was used to encapsulate the electrodes. An arrangement of electrodes was then inserted into the model made of high-quality RTV mould-making silicone rubber (Extreme Silicone) and filled with denture material. After the material had cured, the model was removed from the casting material, inserted into the titanium body of the probe and adhered using medical-grade silicone adhesive (ASC, Applied Silicone Corporation, Part No: 40064, MED RTV adhesive, implant grade, Santa Paula, CA).

When finalized, the area where the effect of NVB stimulation could potentially be produced by the cathode was around 50 mm^2. The geometric surface of both electrodes was enlarged by mechanical grinding with sandpaper (Waterproof Silica Carbide Paper FEPA P#500, Struers ApS, Denmark) to increase irregularity on the cathode surface and thus to decrease the current density at the interface with the NVB tissue. As a result, the $|Z|$ of both electrodes was lowered so they became more suitable for NVB stimulation. Figure 1d shows a stimulation probe with the spiral cathode at the centre of the probe and the ring-shaped anode close to the circumference.

Among the sterilization methods that could be applied with the FEP insulation material, low-temperature hydrogen peroxide gas plasma sterilization was selected.

Assessment of the electrical properties

The $|Z|$ of the electrodes was investigated under simulated physiological conditions in phosphate-buffered saline (PBS) (NaCl, 7.36 g/L; Na_2HPO_4, 11,5 g/L; $NaH_2PO_4 \cdot H_2O$, 3.04 g/L) as a reference. $|Z|$ values at the interface of the cathode and the anode were measured in a chamber filled with PBS using an LCR meter (AT2816A Precision Digital LCR Meter, Changzhou Applent Instruments, Ltd., Jiangsu, China).

In both in vitro and in vivo testing, the stimuli proposed in the paradigm were delivered from the custom-designed nerve stimulator shown in Fig. 2a, which was connected to the voltage booster amplifier shown in Fig. 2c. The corresponding $|Z|$ at the interface of the cathode and the anode in PBS solution versus frequency is shown in Fig. 2d.

The relevant parameters of the stimuli are shown in Table 2. When testing the stimuli, the intensity of the cathodal and anodal parts of the stimulus pulse pair i_c and i_a was identified by measuring the voltage drop across the precision serial resistor at the stimulator output (10 Ω).

Table 2
Stimulation parameters and physical quantities used during testing of the electrical properties of the stimulating probe

Stimulation parameter/physical quantity	**Acronym**	**Value**
Intensity of the cathodal phase (stimulating current)	i_c	10–70 mA
Width of the cathodal phase	t_c	500 μs
Delay between the phases	d	NA
Width of cathodal exponential decay	t_{exp}	300 μs
Time constant of cathodal exponential decay	τ_{exp}	Arbitrary set μs
Intensity of the anodic phase	i_a	10 mA
Width of the anodic phase	t_a	1000 μs
Frequency	f	10 Hz
Cathodal geometric surface	A_c	27 mm^2
Anodal geometric surface	A_a	23 mm^2

Table 3
Electrical quantities and elements that contributed to the voltage drop across the electrode–NVB tissue interface ΔV

Stimulation parameter/physical quantity	Acronym	Value
Stimulating/cathodal charge	Q_c	26 μA s
Anodal charge	Q_a	10 μA s
Cathodal charge density	σQ_c	0.963 μA s/mm^2
Anodal charge density	σQ_a	0.435 μA s/mm^2
Entire voltage drop across the electrode–NVB tissue interface	ΔV	40.4 V
Polarization across the electrode–NVB tissue interface	ΔE_p	24.0149 V
Potential of the cathode at the onset of the stimulating pulse	E_{ipp}	12.53 V
Access voltage (drop across the NVB resistance R_i plus over-potential terms)	V_a	16.38 V
Maximum positive polarization across the electrode–NVB tissue interface	E_{ma}	11.52 V
Maximum negative polarization across the electrode–NVB tissue interface	E_{mc}	−11.49 V

The stimulation/cathodal charge Q_c was calculated as an integral of the surface under the cathodal current i_c between the start and the end of the cathodal part of the stimulus, and nodal charge Q_a was calculated as an integral of the surface under the anodal current i_c between the start and the end of the anodal part of the stimulus.

To identify the potential harm that could occur at the NVB tissue below the cathode during pulsing, cathodal charge density σQ_c was calculated considering the charge at the cathodal part and the geometric surface of the cathode. Similarly, anodal charge density σQ_a was calculated considering the charge at the anodal part and the geometric surface of the anode.

The electrical properties of both the cathode and the anode were studied in vivo using the simple technique of stimulating SVT measurements between the anode and the cathode during RARP while they were in firm contact with the NVB. However, the electrical properties were analysed in one particular stimulating pulse selected from the 5-min train of identical stimulation pulses. Furthermore, $|Z|$ across both the cathode-NVB tissue and the anode-NVB tissue was determined to investigate the electrical properties of the cathode and anode under in vivo physiological conditions. $|Z|$ was calculated from the current i_c flowing between the cathode and anode through the NVB tissue and the SVT that developed

between the cathode and anode during NVB stimulation [44]. E_{mc} and E_{ma} were defined across the electrode–NVB tissue interface. These potentials were then tested to establish if any exceeded the values confining the water electrolysis window defined by the cyclic voltammetry CV values [− 0.60 V, + 0.85 V] measured in PBS [53]. The stimulation parameters, physical quantities, their values and acronyms that were used/delivered during testing of the electrical properties of the stimulating probe are presented in Table 2.

Assessment of the physiological properties

Five patients (mean age, 57 years) scheduled for RARP were enrolled in the study. All were confirmed to have clinically localized prostate cancer (stage T1 or T2). After being informed about the purpose and procedures of the study, they provided written informed consent.

Before the surgery, the probe was introduced into the operating field through the fifth lateral port (AirSeal), and lead wires remained in part within the port and in part outside the port to allow connection to the stimulator output. During the sparing procedure, the NVBs were carefully removed and isolated from the prostate and freed from excessive fat tissue in preparation for testing the physiological performance.

The probe was then placed in the middle of the NVB for 5 min, once on the left side and once on the right side [19]. NVB stimulation was delivered via stimulation electrodes connected to the custom-designed nerve stimulator when the parameters identified in Table 1 were predefined via dials by the principal investigator. Based on the above-mentioned paradigm, i_c was adjusted to 50 mA after firm contact of the probe was established by the surgeon. It was necessary to activate predominant non-myelinated NVB fibres located at a certain distance from the stimulating electrodes, therefore firm contact of the probe is crucial to deliver a stimulating charge onto the NVB at a density not harmful to the NVB tissue.

A multi-sensorial device combining commercial and custom-crafted sensors was developed to monitor and evaluate eventual penile erectile events. The main parts of the device to measure penile axial rigidity involve a set of 4 different-sized custom-developed bell-shaped probes and a tensile/compressive force transducer (Type S2, Hottinger Brüel & Kjær GmbH, Darmstadt, Germany). Before the measurements, the appropriate size of the bell-shaped probe was selected for each patient and mounted onto the multisensorial device.

For the study of smooth muscle activity within the penile shaft, dual-channel CC-EMG measurements were performed using a high-performance general-purpose amplifier (ETH-256 2-Channel Bridge/ECG/EMG/EEG/Bio-Amplifier, iWorx/CB Sciences, Dover, DE) with the following settings: gain, ×100; low-pass filter, 50 Hz; high-pass filter, 0.03 Hz. A 3-lead isolated biopotential recording preamplifier (C-ISO-256, iWorx/CB Sciences, Dover, DE) was used to provide galvanical isolation between the patient and the ETH-256 with the following settings: gain, ×400; high-pass filter, 0.05 Hz; low-pass filter, 2500 Hz. CC-EMG was measured between the base and the tip region of the penis using surface and subdermal

needle electrodes [19]. Intracavernosal CC-EMG was measured with platinum-iridium disposable needle electrodes (TE/S46-638; Technomed Europe, Maastricht-Airport, The Netherlands) connected to positive inputs of the recording preamplifier. They were inserted at the 3 o'clock position into the middle of the left CC penile shaft and at the 9 o'clock position into the middle of the right CC penile shaft. Their tips were positioned around the centre of the CCs. For surface CC-EMG measurements, however, 2 pre-gelled 20-mm disposable silver and silver chloride electrodes (Ag/AgCl) (part number 019-400400; Natus, Middleton, WI) were placed on the left CC shaft at the 5 o'clock position and on the right CC shaft at the 7 o'clock position as close as possible to the proximal part of the penis [19]. One pair of surface and subdermal needle electrodes was placed on the left and another on the right pubis to serve as a ground for the CC-EMG signals.

Data acquisition and offline signal analysis

The data were gathered at a sampling rate f_s=200.00 kHz/channel with 24-bit resolution using a high-performance I/O data acquisition system (DEWE-43a; Dewesoft d. o. o., Trbovlje, Republic of Slovenia) and data acquisition software (DewesoftX). The stimulation intensity i_c was assessed by measuring the voltage drop across the precision serial 10 Ω resistor connected to the stimulator output. During the acquisition, the CC-EMGr and CC-EMGr signals were filtered and stored on a portable computer (Lenovo W541, Lenovo, Beijing, China). Offline signal analysis was performed using MATLAB R2024b software (Mathworks Inc., Natick, MA).

Recordings of i_c and SVT were analysed after a reconstructed NVB stimulation duration (NVB_{sd}) of 305.77 s. The DC component was then removed from i_c and SVT, and the corresponding spectral density was calculated using MATLAB Welch's power spectral density estimate. The absolute impedance $|Z|$ was calculated simply by dividing the spectral density of i_c and SVT. With regard to the analysis of the CC-EMG recordings, frequency spectral cumulative curves (amplitude and power spectrum curves) were calculated for the right ($CC\text{-}EMG_r$) and left ($CC\text{-}EMG_l$). An amplitude cumulative curve represents the sum of the amplitudes of spectral components, and a power spectrum cumulative curve represents the sum of the powers of spectral components.

Results

Assessment of electrical properties

A stimulation current pulse with a cathodal intensity of i_c = − 50 mA and the resulting SVT are shown in Fig. 3. The SVT trace represents the waveform of the voltage difference between the cathode and anode during injection of a stimulating current i_c. There were also several elements shown in Fig. 3 that contributed to the entire voltage drop (ΔV), and they were accounted for in the calculation of E_{mc} and E_{ma}: ΔE_p, polarization across the electrode–electrolyte interface; E_{ipp}, potential of the cathode at the

onset of the pulse; and V_a, access voltage (drop across the electrolyte resistance R_i plus over-potential terms). The values of these elements read from the SVT trace are presented numerically in Table 4. The table also shows Q_c and Q_a, as well as the corresponding cathodal (σQ_c) and anodal (σQ_a) charge density. E_{mc} is defined by Eq. (1) [53, 54]; ΔE_p was obtained by subtraction of V_a from the measured voltage drop ΔV.

$$E_{mc} = E_{ipp} + \Delta E_p = E_{ipp} + (\Delta V - V_a) = 12.53\ V - (40.4 - 16.38)\ V = -11.49\ V \quad (1)$$

The value of E_{ma}, also read from the SVT trace shown in Fig. 4, was 11.52 V.

Figure 4 shows the absolute $|Z|$ calculated using the frequency domain Fourier analysis method. This method was used because it provided a more accurate estimation of $|Z|$ than the time domain method, especially when recordings contain both pulses and noise.

Assessment of physiological properties

Figure 5. shows the CC-EMG records in the left and right CC and the amplitude and power spectrum cumulative curves for both CC-EMGs in one of the 5 patients (GM) while the left and right NVB were stimulated. Figure 5a shows i_c (top trace), CC-EMGr (intermediate trace) and CC-EMGl while the left NVB was stimulated. Figure 5b shows the amplitude and power spectrum cumulative curves for CC-EMGr. Figure 5c shows i_c (top trace), CC-EMGr (intermediate trace) and CC-EMGl while the right NVB was stimulated. Figure 5d shows the amplitude and power spectrum cumulative curves for CC-EMGl.

Discussion

The present article reviews the electrical and physiological properties of the electrode–NVB tissue interface for stimulation electrodes within the probe to be used in NVB stimulation during RARP. The goal of the study was to develop and test the paradigm and stimulation system for efficient and selective NVB stimulation to elicit erectile events during RARP. The study focused on testing the hypothesis that stimulating electrodes within the probe and predefined stimulating pulses are appropriate for effective NVB stimulation. A quantitative description of the stimulating electrode–NVB tissue interface from the in vivo measurements has been documented. The ultimate goal of the study was to assess the status of NVB preservation by the surgeon's judgement during the operation and the changes in CC-EMG related to NVB stimulation. The surgeon should correctly identify the NVB to ensure exact preservation and avoid injury to the NVB during RARP [1–4]. For this purpose, bilateral nerve-sparing procedures were performed in the 5 patients enrolled in the study.

Assessment of electrical properties

The most significant results on testing the electrical properties of the probe are shown graphically in Fig. 3, as well as the relation between the stimulation pulse and elicited SVT and elements that

contributed to the entire voltage drop ΔV across the interface between the cathode and the anode and NVB tissue. The numerical values of the electrical quantities and elements from Fig. 3 are presented in Table 4. A practical issue in determining E_{mc} was the difficulty in accurately measuring V_a. As shown in Fig. 3, the onset of i_c elicited near-instantaneous voltage, so that V_a could be easily determined. However, when i_c was terminated, the behaviour of the potential in the exponential decay region, where i_c approached the lowest value, meant that V_a could not be determined easily [53, 54] because exponential decay plays a specific role. However, E_{ma} was determined with relative ease. As seen in the SVT, E_{mc} and E_{ma} reached − 11.49 V and 11.52 V, respectively. It was also noticed that V_a and ΔE_p were not the same value (Fig. 3).

The in vivo impedance $|Z|$ of the stimulation electrodes was determined mainly by the actual area of the cathode and the anode that was obtained by mechanical grinding during fabrication [26]. Thus, a surface of the cathode modified with rough sandpaper could deliver more current to the NVB tissue and provide more activation for a fixed input voltage. As the total i_c delivered was reduced, activation was obtained at a reduced input power. $|Z|$ decreased exponentially from high values at low frequencies to low values at high frequencies (Fig. 4), thus indicating the pure capacitive nature of the electrode–NVB tissue interface. It was also shown that coherence between i_c and SVT was near 1, indicating that they were strongly connected.

The original question was how to develop stimulation electrodes and a stimulation pulse to enable safe and efficient NVB stimulation at the same time. The greatest concern in deciding on the dimensions of the cathode and the anode was to avoid an electrochemical regimen such that charge injection during NVB stimulation would not remain within reversible limits. The results show that there was a circumstance when the stimulation electrodes operated in a regimen whereby potentials were pushed outside the safe region. Electrochemical reactions that occurred at the cathode owing to the charge Q_c injected via the cathodal phase were not completely reversed by the charge Q_a injected via the anodic phase [14, 24, 28].

Accordingly, the data on the electrical properties of the probe only partly support our hypothesis. Namely, E_{mc} and E_{ma} largely exceed the safe potential limits of water electrolysis [0.60 V, + 0.85 V]. This is not a desirable property of clinical stimulation electrodes because, in conditions where Faradaic charge transfer predominates over capacitive charge transfer, chemical reactions may occur [24, 28, 29]. Fortunately, the NVB stimulations were not permanent and lasted only 5 min for the left and right NVB.

As more becomes known about RARP, it is necessary to provide a basis for the choice of materials and the design of stimulating electrodes for NVB stimulation. To reveal certain quantitative information about the anode– and cathode–NVB tissue interface and limits of the stimulation pulses, the electrochemical techniques deployed were selected based on their ability to enable short-term selective and safe NVB stimulation. The results on the electrical performance of the electrode–NVB tissue interface were consistent with reports from other investigators [22, 24–26, 29]. To stimulate a certain

group of NVB fibres and avoid injury associated with a high charge density, NVB stimulation started only when firm contact of the stimulation electrodes and the location was made so that the i_c was delivered at the lowest density and lowest impedance |*Z*|. Such conditions were expected because the parameters of the stimulation pulses that were applied to the NVB tissue to depolarize non-myelinated nerve fibres were relatively high.

The results show that both in vitro and in vivo, low frequencies during pulsing resulted in significant differences in measured |*Z*|. Due to the different conditions at the 2 interfaces, |*Z*| at 50 Hz was 170 Ω in vitro and 1500 Ω in vivo. However, aiming to obtain |*Z*| of the interface only between stimulation electrodes and NVB tissue, a resistivity of 22.26 Ω (12.26 Ω leading wires, 10 Ω measurement resistor) must be deducted from the measured valus of |*Z*|. Furthermore, |*Z*| during pulsing in vitro lowered faster with increasing frequency than during pulsing in vivo due to a much larger number and greater mobility of ionic carriers available in the in vitro environment.

Our further work could test different stimulation waveforms and parameters to answer the questions raised by our results with regard to the electrical properties of the probe.

Assessment of physiological properties

As shown in Fig. 5a and c, NVB stimulation elicited high-quality CC-EMG waveforms in all our patients. In the upper trace in Fig. 5a, the amplitude of CC-EMGr, which was recorded from the right CC at the start of an 85-s-long left NVB stimulation, can be seen to be lower than that of CC-EMGl, which was recorded from the left CC. Within the next 80 s, when the left NVB was stimulated with intensity i_c=70 mA, the CC-EMGr amplitude recorded from the right CC was also lower than the CC-EMGl recorded from the left CC. Within the remaining 135 s, when the left NVB was stimulated with the same intensity i_c=70 mA, the CC-EMG amplitude recorded from the right and left CC was the highest and almost the same. Within this time period, the appearance of both CC-EMG waves was synchronized.

However, Fig. 5c (upper trace) shows that with right NVB stimulation with intensity i_c=60 mA for the entire time period of 300 s, the CC-EMGr amplitude recorded from the right CC was roughly the same as the CC-EMGl recorded from the left CC. Within this time period, both CC-EMG waves appeared almost synchronized.

The results do not confirm the original question of whether it is possible to selectively stimulate fibre populations of different types and different diameters within the NVB. Any effect indicating faster, stronger and more durable erections based on activation of a preferential population of C-fibres in an NVB could not be identified.

Therefore, the hypothesis proposing fibre-type selective NVB stimulation tested by exploiting the difference in the threshold between different nerve fibre diameters has not been confirmed. However, the ability of the electrodes to activate a certain volume of NVB tissue with as low as possible voltage and power requirements, an important desire [26, 28], was confirmed. The results also show that NVB

stimulation is strongly dependent on the physical proximity of the electrodes deployed and the distance between the electrodes and the NVB tissue [29, 48, 52].

The results on the physiological properties of the electrodes were consistent with reports from other investigators [31, 55, 56]. This may be seen in Fig. 5, which shows CC-EMG signals recorded in the left and right CC just after RARP while the left and right NVBs were stimulated. All 4 CC-EMG traces were of high quality and, as such, they confirmed the functionality of the isolated NVB tissue [41, 44, 45]. However, the measurements were accomplished in patients with satisfactory EF pre-operatively. With regard to the assessment of other physiological properties of the probe, no increase in axial rigidity was obtained in any of the assessments. This outcome is in contrast to outcomes published in the literature [3, 5, 36, 44]. One possible reason for the absence of axial rigidity could be constriction of blood vessels due to NVB stimulation [57]. Another possible reason for the lack of erectile responses may include the limited time allocated for NVB stimulation.

Nevertheless, the surface area of the stimulation cathode may not have been able to establish effective electrical contact with a sufficient number of NVB neural fibres. The extent and neurological outcome of these effects on EF are not known and should be assessed in further research [58].

One parameter for a quasi-trapezoidal pulse that might be important for confirmation of the paradigm is the arbitrarily preset τ_{exp}. Its precise influence on EF was not identified. It could only be speculated that the AP of the Aδ-fibres were not blocked, whereas the AP of the C-fibres passed through.

One method that might be used to confirm or discredit the proposed paradigm is CC-EMG [42, 59]. CC-EMG features in the frequency domain were computed from an NVB stimulation duration (NVB_{sd}) of 305.77 s. The amplitude and power spectrum cumulative curve computed is shown in Fig. 5b for CC-EMGr and in Fig. 5d for CC-EMGl. The median frequency (MF) is an indicator of the CCM status under NVB stimulation conditions. It is obtained from the amplitude and power spectrum cumulative curves of a recorded CC-EMG [47]. Reasons for changes in the CC-EMG are modulation of the recruitment firing rate, grouping and slowing of the CV and synchronization of the signal. The MF in the amplitude cumulative curve in Fig. 5b was 26.7 Hz, and the MF in the power spectrum cumulative curve was 50 Hz. Furthermore, the MF in the amplitude cumulative curve shown in Fig. 5d was 28.23 Hz and the MF in the power spectrum cumulative curve was 43.58 Hz. It may be seen in the cumulative curves of both CC-EMGs that they were contaminated with harmonics that came from the NVB stimulation pulses and with frequency that came from the facility mains.

Results for the physiological properties from the assessment probe also showed that no measurable increases in penile axial rigidity were observed in response to NVB stimulation in any of the patients.

Further research should consider even longer NVB stimulation periods to obtain a more consistent picture on the status of the NVB tissue just after RARP. Further improvement in the NVB stimulation scheme, including different patterns of stimulation pulses, will be implemented to elicit measurable axial

rigidity during NVB stimulation. In addition, a probe with a larger and modified area of stimulating electrodes will be crafted.

Conclusion

The results suggest that CC-EMG may provide valuable intraoperative feedback regarding the functional integrity of NVBs during RARP. However, no immediate measurable changes in EF parameters, such as axial rigidity, were observed after NVB stimulation, highlighting the complexity of real-time intraoperative assessment of EF. The results show that the design of the stimulating electrodes, based on the electrical properties of the real area of the cathode and properties of NVB nerve fibres, could be useful for the development of probes for NVB stimulation.

If successfully developed further, the paradigm would enable significant improvement of current NVB sparing during RARP. A preference towards nerve fibre-type NVB stimulation may be advantageous for eliciting adequate EF during RARP and for preserving sexual function after RARP. However, more detailed investigations of neural control systems, considering the realistic structural topography of the NVB and the presence of a spatio-temporal constraint based on the electrophysiology of unmyelinated C-fibres, should be carried out based on this work.

Declarations

Ethics approval

This study was performed in line with the principles of the Declaration of Helsinki. Approval was granted by the National Medical Ethics Committee, Ministry of Health, Republic of Slovenia (2 July, 2024/no. 0120–138/2024-2711-6).

Consent to participate

Informed consent was obtained from all participants in the study.

Funding

This work was supported in part by Slovenian Research and Innovation Agency (grant number P3-0171) and in part by University Medical Centre Ljubljana (grant number 292401).

Competing interests

The authors have no relevant financial or non-financial interests to disclose.

Author Contribution

J.R. Developed the model for selective NVB stimulation, methods, hardware and wrote the manuscript. J.B. Performed surgery and CC-EMG measurements.T.S. Revised the research methods.S.R. Assisted with interpreting the data, discussed the results and commented on the manuscript.S.H. Perfomed surgery and NVB stimulation.

Acknowledgements

The authors would like to thank members of the team in the surgical facility for their assistance with the experiments.

References

1. University of Florida Health Robotic nerve-sparing radical prostatectomy. https://urology.ufl.edu/patient-care/robotic-laparoscopic-urologic-surgery/procedures/robotic-nerve-sparing-radical-prostatectomy/
2. Biology Insights Cavernous nerve function damage and rehabilitation. https://biologyinsights.com/cavernous-nerve-function-damage-and-rehabilitation/
3. Nguyen LN, Head L, Witiuk K, Punjani N, Mallick R, Cnossen S, Fergusson DA, Cagiannos I, Lavallée LT, Morash C, Breau RH (2017) The risks and benefits of cavernous neurovascular bundle sparing during radical prostatectomy: a systematic review and meta-analysis. J Urol 198(4):760–769. https://doi.org/10.1016/j.juro.2017.02.3344
4. O'Neil B, Koyama T, Alvarez J, Conwill RM, Albertsen PC, Cooperberg MR, Goodman M, Greenfield S, Hamilton AS, Hoffman KE, Hoffman RM, Kaplan SH, Stanford JL, Stroup AM, Paddock LE, Wu XC, Stephenson RA, Resnick MJ, Barocas DA, Penson DF (2016) The comparative harms of open and robotic prostatectomy in population based samples. J Urol 195(2):321–329. https://doi.org/10.1016/j.juro.2015.08.092
5. Mulhall JP, Bivalacqua TJ, Becher EF (2013) Standard operating procedure for the preservation of erectile function outcomes after radical prostatectomy. J Sex Med 10(1):195–203. https://doi.org/10.1111/j.1743-6109.2012.02885.x
6. Goodman M, Greenfield S, Hamilton AS, Hoffman KE, Hoffman RM, Kaplan SH, Stanford JL, Stroup AM, Paddock LE, Wu X-C, Stephenson RA, Resnick MJ, Barocas DA, Penson DF (2016) The comparative harms of open and robotic prostatectomy in population based samples. J Urol 195:321–329. https://doi.org/10.1016/j.juro.2015.08.092
7. Lepor H, Gregerman M, Crosby R, Mostofi FK, Walsh PC (1985) Precise localization of the autonomic nerves from the pelvic plexus to the corpora cavernosa: a detailed anatomical study of the adult male pelvis. J Urol 133(2):207–212. https://doi.org/10.1016/s0022-5347(17)48885-9
8. Jung J, Jo HW, Kwon H, Jeong NY (2014) Clinical neuroanatomy and neurotransmitter-mediated regulation of penile erection. Int Neurourol J 18(2):58–62. https://doi.org/10.5213/inj.2014.18.2.58

9. Auffenberg GB, Pariser JJ, Helfand BT (2016) Normal erectile physiology. In: Köhler T, McVary K (eds) Contemporary treatment of erectile dysfunction. Contemporary endocrinology. Humana, Cham. https://doi.org/10.1007/978-3-319-31587-4_2
10. Rodrigues TM, Mitre AI, da Silva LFF, Castilho LN, Simões FA, Saldiva PHN, Srougi M (2017) Periprostatic innervation: new issues based on segmental analysis of 10 human cadaver pelvic blocs. Prostate 77(10):1151–1159. https://doi.org/10.1002/pros.23374
11. Tode J, Kirillova-Woytke I, Rausch VH, Baron R, Jänig W (2018) Mechano- and thermosensitivity of injured muscle afferents 20 to 80 days after nerve injury. J Neurophysiol 119(5):1889–1901. https://doi.org/10.1152/jn.00894.2017
12. Takenaka A, Soga H, Hinata N, Honda M, Sejima T, Muramaki M, Miyake H, Tanaka K, Fujisawa M (2011) Classification of the distribution of cavernous nerve fibers around the prostate by intraoperative electrical stimulation during laparoscopic radical prostatectomy. Int J Impot Res 23(2):56–61. https://doi.org/10.1038/ijir.2011.4
13. Butson CR, Miller IO, Normann RA, Clark GA (2011) Selective neural activation in a histologically derived model of peripheral nerve. J Neural Eng 8(3):036009. https://doi.org/10.1088/1741-2560/8/3/036009
14. Pečlin P, Rozman J (2014) Alternative paradigm of selective vagus nerve stimulation tested on an isolated porcine vagus nerve. ScientificWorldJournal 2014:310283. https://doi.org/10.1155/2014/310283
15. Gasser HS (1941) The classification of nerve fibers. Ohio J Sci 41(3):145–159
16. Arcilla CK, Tadi P (2026) Neuroanatomy, unmyelinated nerve fibers. StatPearls [Internet]. Treasure Island (FL)
17. Furrer MA, Sathianathen N, Gahl B, Wuethrich PY, Giannarini G, Corcoran NM, Thalmann GN (2023) Functional impact of neuro-vascular bundle preservation in high risk prostate cancer without compromising oncological outcomes: a propensity-modelled analysis. Cancers (Basel) 15(24):5839. https://doi.org/10.3390/cancers15245839
18. Shafik A (1994) Cavernous nerve stimulation through an extrapelvic subpubic approach: role in penile erection. Eur Urol 26(1):98–102. https://doi.org/10.1159/000475351
19. Song WH, Park JH, Tae BS, Kim SM, Hur M, Seo JH, Ku JH, Kwak C, Kim HH, Kim K, Jeong CW (2020) Establishment of novel intraoperative monitoring and mapping method for the cavernous nerve during robot-assisted radical prostatectomy: results of the phase I/II, first-in-human, feasibility study. Eur Urol 78(2):221–228. https://doi.org/10.1016/j.eururo.2019.04.042
20. Hyun SE, Kim K (2021) Intra-operative cavernous nerve monitoring and mapping during radical prostatectomy: a case report of corpus cavernosum electromyography. J Intraoper Neurophysiol 3(2):97–101. https://doi.org/10.33523/join.2021.3.2.97
21. Tsujimura A, Miyagawa Y, Takao T, Matsumiya K, Nakayama M, Tsujimoto Y, Takaha N, Nishimura K, Nonomura N, Takada T, Fujioka H, Kurokawa K, Aozasa K, Okuyama A (2006) Significance of

electrostimulation in detecting neurovascular bundle during radical prostatectomy. Int J Urol 13(7):926–931. https://doi.org/10.1111/j.1442-2042.2006.01442.x

22. Stevenson M, Baylor K, Netherton BL, Stecker MM (2010) Electrical stimulation and electrode properties. Part 2: pure metal electrodes. Am J Electroneurodiagnostic Technol 50(4):263–296. https://doi.org/10.1080/1086508X.2010.11079783
23. Barr RC, Plonsey R (1995) Threshold variability in fibers with field stimulation of excitable membranes. IEEE Trans Biomed Eng 42(12):1185–1191. https://doi.org/10.1109/10.476125
24. Brummer SB, Turner MJ (1997) Electrochemical considerations for safe electrical stimulation of the nervous system with platinum electrodes. IEEE Trans Biomed Eng 24(1):59–63. https://doi.org/10.1109/TBME.1977.326218
25. McCreery DB, Agnew WF, Yuen TG, Bullara L (1990) Charge density and charge per phase as cofactors in neural injury induced by electrical stimulation. IEEE Trans Biomed Eng 37:996–1001. https://doi.org/10.1109/10.102812
26. Golestanirad L, Elahi B, Molina A, Mosig JR, Pollo C, Chen R, Graham SJ (2013) Analysis of fractal electrodes for efficient neural stimulation. Front Neuroeng 6:3. https://doi.org/10.3389/fneng.2013.00003
27. Warman EN, Grill WM, Durand D (1992) Modeling the effects of electric fields on nerve fibers: determination of excitation thresholds. IEEE Trans Biomed Eng 39(12):1244–1254. https://doi.org/10.1109/10.184700
28. Rose TL, Robblee LS (1990) Electrical stimulation with Pt electrodes: VIII. Electrochemically safe charge injection limits with 0.2 ms pulses. IEEE Trans Biomed Eng 37:1118–1120. https://doi.org/10.1109/10.61038
29. Geddes LA, Roeder R (2003) Criteria for the selection of materials for implanted electrodes. Ann Biomed Eng 31(7):879–890. https://doi.org/10.1114/1.1581292
30. Regnacq L, Giraud R, Ortega Sanabria A, Thota A, Roversi L, Rouhani M, McPherson L, Abbas JJ, Jung R, Romain O, Renaud S, Bornat Y, Kolbl F (2021) Evaluation of stimulation waveforms for safe and efficient peripheral nervous system activation. In: 2021 Biomedical Circuits and Systems Conference (BioCAS 2021): Restoring vital functions by electronics-achievements, limitations, opportunities, and challenges. IEEE, Berlin, Germany. https://hal.science/hal-03542068v1
31. Geddes LA (1997) Historical evolution of circuit models for the electrode–electrolyte interface. Ann Biomed Eng 25:1–14. https://doi.org/10.1007/BF02738534
32. Merrill DR (2010) The electrochemistry of charge injection at the electrode/tissue interface. In: Zhou D, Greenbaum E (eds) Implantable neural prostheses 2. Biological and medical physics, biomedical engineering. Springer, New York, pp 85–138. https://doi.org/10.1007/978-0-387-98120-8_4
33. Pour Aryan N, Kaim H, Rothermel A (2025) Electrode materials: state-of-the-art and experiments. In: Pour Aryan N, Kaim H, Rothermel A (eds) Stimulation and recording electrodes for neural prostheses, vol 78. Springer, Cham, pp 45–64. https://doi.org/10.1007/978-3-319-10052-4

34. Boehler C, Carli S, Fadiga L, Stieglitz T, Asplund M (2020) Tutorial: guidelines for standardized performance tests for electrodes intended for neural interfaces and bioelectronics. Nat Protoc 15(11):3557–3578. https://doi.org/10.1038/s41596-020-0389-2
35. Jönsson EH, Backlund Wasling H, Wagnbeck V, Dimitriadis M, Georgiadis JR, Olausson H, Croy I (2025) Unmyelinated tactile cutaneous nerves signal erotic sensations. J Sex Med 12(6):1338–1345. https://doi.org/10.1111/jsm.12905
36. Klotz L, Herschorn S (1998) Early experience with intraoperative cavernous nerve stimulation with penile tumescence monitoring to improve nerve sparing during radical prostatectomy. Urology 52(4):537–542. https://doi.org/10.1016/s0090-4295(98)00319-7
37. Wagner G, Gerstenberg T, Levin RJ (1989) Electrical activity of corpus cavernosum during flaccidity and erection of the human penis: a new diagnostic method? J Urol 142(3):723–725. https://doi.org/10.1016/s0022-5347(17)38867-5
38. Stief CG, Thon WF, Djamilian M, Allhoff EP, Jonas U (1992) Transcutaneous registration of cavernous smooth muscle electrical activity: noninvasive diagnosis of neurogenic autonomic impotence. J Urol 147(1):47–50. https://doi.org/10.1016/s0022-5347(17)37130-6
39. Sasso F, Gulino G, Alcini E (1996) Corpus cavernosum electromyography (CC-EMG): a new technique in the diagnostic work-up of impotence. Int Urol Nephrol 28(6):805–818. https://doi.org/10.1007/BF02550732
40. Merckx LA, de Bruyne RM, Keuppens FI (1993) Electromyography of cavernous smooth muscle during flaccidity: evaluation of technique and normal values. Br J Urol 72(3):353–588. https://doi.org/10.1111/j.1464-410X.1993.tb00732.x
41. Vírseda-Chamorro M, Lopez-Garcia-Moreno AM, Salinas-Casado J, Esteban-Fuertes M (2012) Usefulness of electromyography of the cavernous corpora (CC EMG) in the diagnosis of arterial erectile dysfunction. Int J Impot Res 24(4):165–169. https://doi.org/10.1038/ijir.2012.10
42. Leddy LS, Jiang X, Gottsch HP, Yang CC (2012) Corpus cavernosum electromyography revisited: defining the origin of the signal. J Urol 187:589–593. https://doi.org/10.1016/j.juro.2011.09.157
43. Yildiz A, Islamogl E, Yuksel M, Erol I, Karamik K, Cakir T, Ates M, Savas M (2021) Assessment of changes in penile sensation by electrophysiological study after radical prostatectomy: a pilot study. Curr Urol 15(2):111–114. https://doi.org/10.1097/CU9.0000000000000016
44. European Commission (2005) Corpus cavernosum EMG in erectile dysfunction. COST Action B18 final report. Period: from 12-2000 to 04-2005. https://cordis.europa.eu/project/id/B18/de
45. Jiang XG, Speel TGW, Wagner G, Meuleman EJH, Wijkstra H (2003) The value of corpus cavernosum electromyography in erectile dysfunction: current status and future prospect. Eur Urol 43(3):211–218. https://doi.org/10.1016/s0302-2838(03)00011-3
46. Pozzo M, Farina D, Merletti R (2004) Electromyography: detection, processing and applications. In: Moore J, Zouridakis G (eds) Biomedical technology and devices handbook. CRC, Boca Raton, FL
47. Phinyomark A, Thongpanja S, Hu H, Phukpattaranont P, Limsakul C (2012) The usefulness of mean and median frequencies in electromyography analysis. In: Naik GR (ed) Computational intelligence

in electromyography analysis-a perspective on current applications and future challenges. Intech. https://dx.doi.org/10.5772/50639

48. McNeal DR (1976) Analysis of a model for excitation of myelinated nerve. IEEE Trans Biomed Eng 23:329–337. https://doi.org/10.1109/TBME.1976.324593
49. Rattay F (1989) Analysis of models for extracellular fiber stimulation. IEEE Trans Biomed Eng 36:676–682. https://doi.org/10.1109/10.32099
50. Accornero N, Bini G, Lenzi GL, Manfredi M (1977) Selective activation of peripheral nerve fibre groups of different diameter by triangular shaped stimulus pulses. J Physiol 273:539–560. https://doi.org/10.1113/jphysiol.1977.sp012109
51. Fukushima K, Yahara O, Kato M (1975) Differential blocking of motor fibers by direct current. Pflugers Arch 398:235–242. https://doi.org/10.1007/BF00587220
52. Fang Z-P, Mortimer JT (1991) Selective activation of small motor axons by quasitrapezoidal current pulses. IEEE Trans Biomed Eng 38(2):168–174. https://doi.org/10.1109/10.76383
53. Hudak EM, Mortimer JT, Martin HB (2010) Platinum for neural stimulation: voltammetry considerations. J Neural Eng 7(2):26005. https://doi.org/10.1088/1741-2560/7/2/026005
54. Cogan SF (2008) Neural stimulation and recording electrodes. Annu Rev Biomed Eng 10:275–309. https://doi.org/10.1146/annurev.bioeng.10.061807.160518
55. Gorman PH, Mortimer JT (1983) The effect of stimulus parameters on the recruitment characteristics of direct nerve stimulation. IEEE Trans Biomed Eng 30(7):407–414. https://doi.org/10.1109/tbme.1983.325041
56. Wei XF, Grill WM (2009) Analysis of high-perimeter planar electrodes for efficient neural stimulation. Front Neuroeng 2:15. https://doi.org/10.3389/neuro.16.015.2009
57. Kezurer N, Farah N, Mandel Y (2016) Endovascular electrodes for electrical stimulation of blood vessels for vasoconstriction – a finite element simulation study. Sci Rep 6:31507. https://doi.org/10.1038/srep31507
58. Ponseti J, Bosinski HA (2010) Brain potentials related to corpus cavernosum electromyography. Int J Impot Res 22(3):171–178. https://doi.org/10.1038/ijir.2010.5

Figures

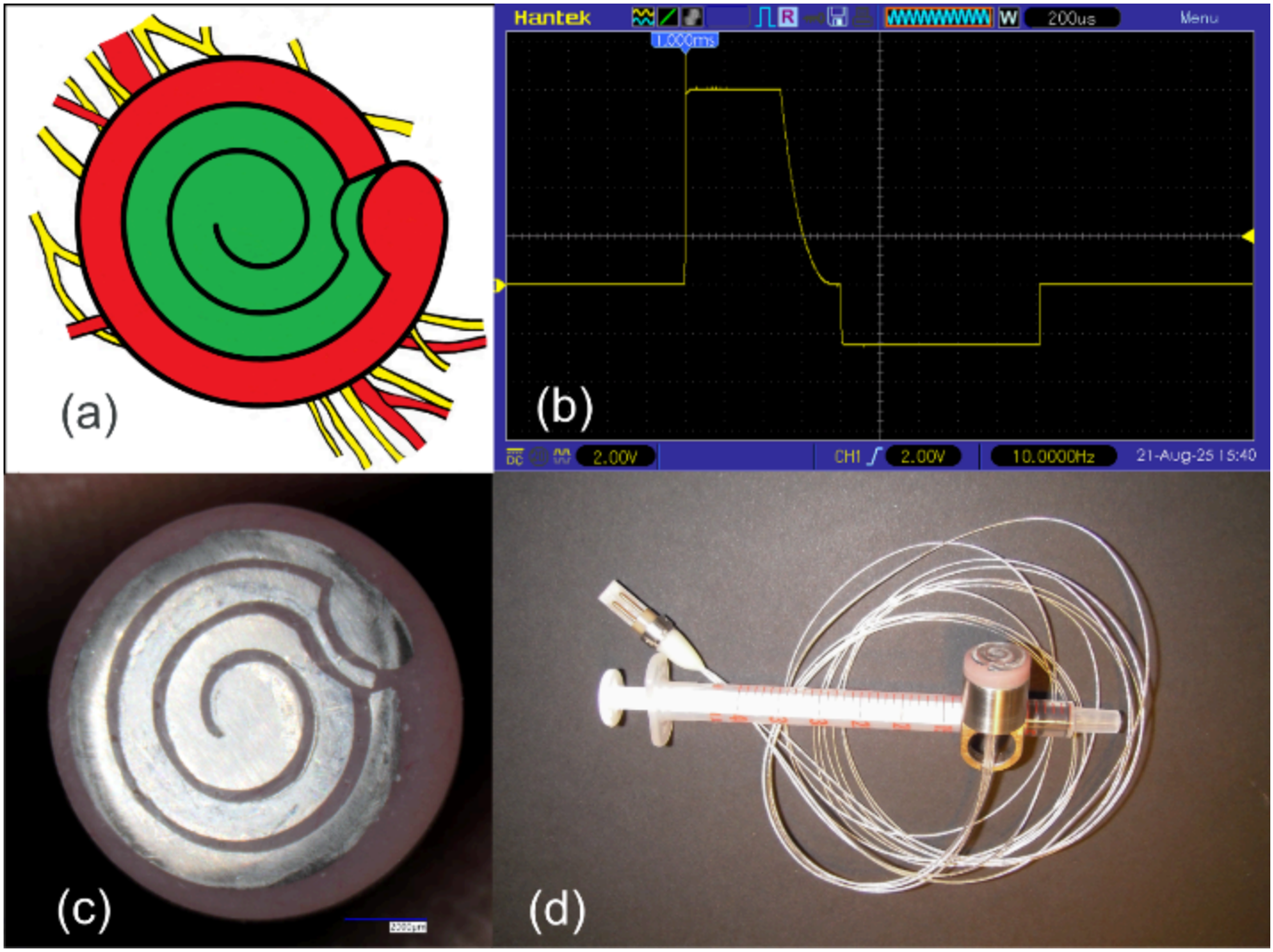


Figure 1

Components of the paradigm for selective NVB stimulation. (a) Schematic diagram of the cathode and the anode above the NVB nerves and blood vessels. (b) Waveform of the quasi-trapezoidal stimulating pulse. (c) Arrangement, shape and dimensions of the cathode and the anode. (d) Probe

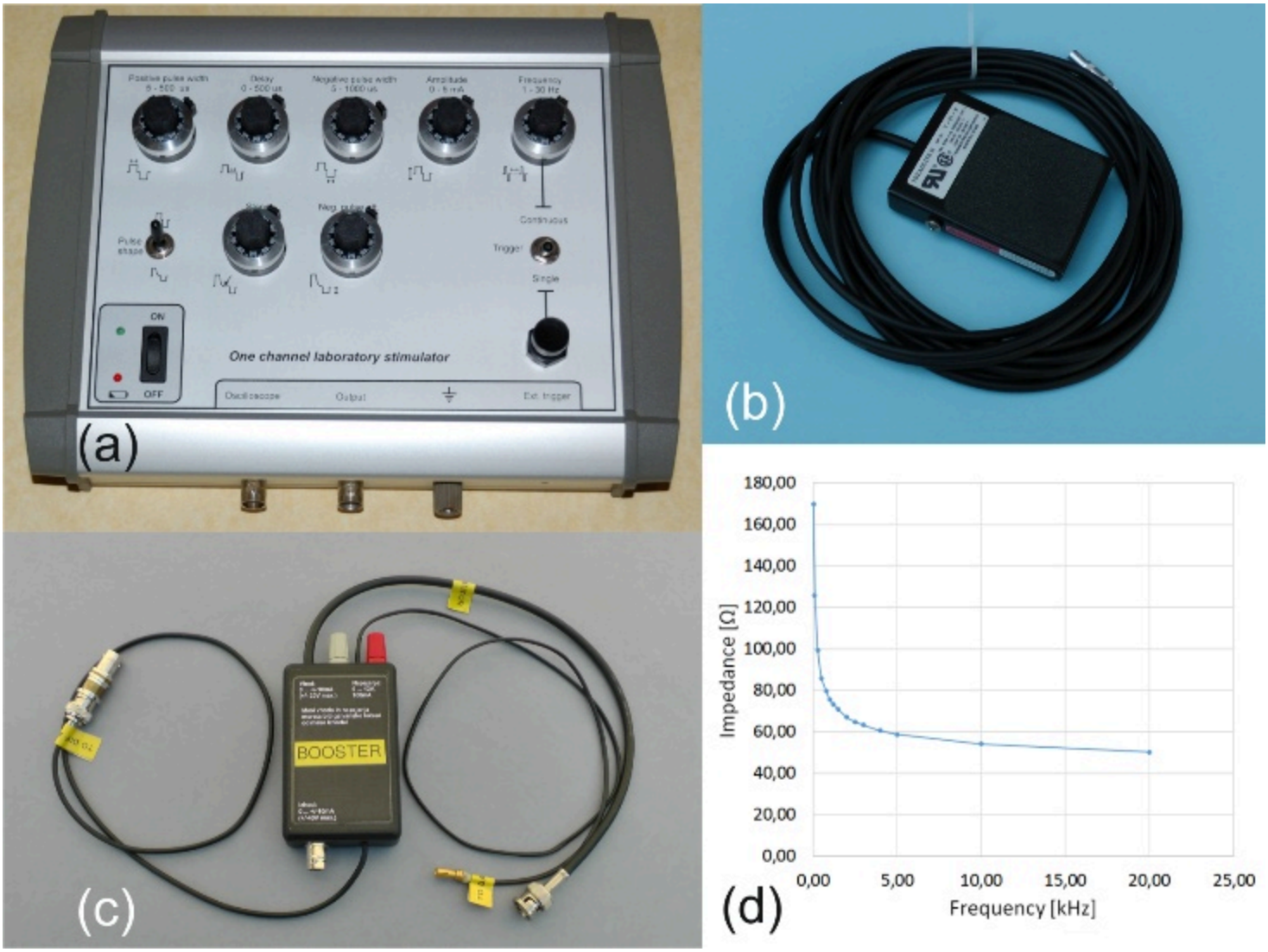


Figure 2

(a) Nerve stimulator. (b) Foot switch. (c) Voltage booster amplifier. (d) |*Z*| at the interface of the cathode and the anode in PBS

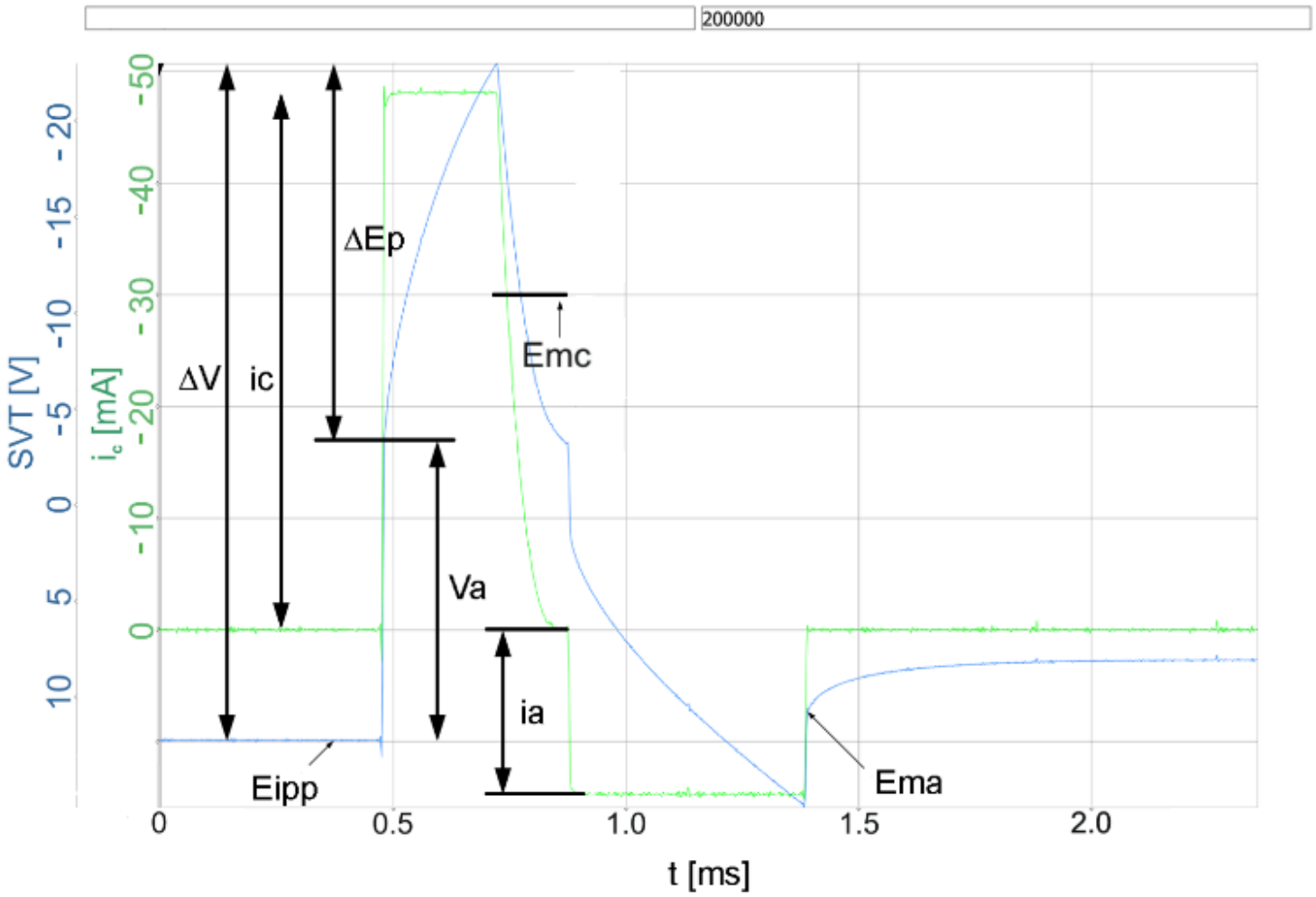


Figure 3

Stimulation pulse and elicited SVT in the cathode with indicated elements that contributed to the entire voltage drop Δ*V*

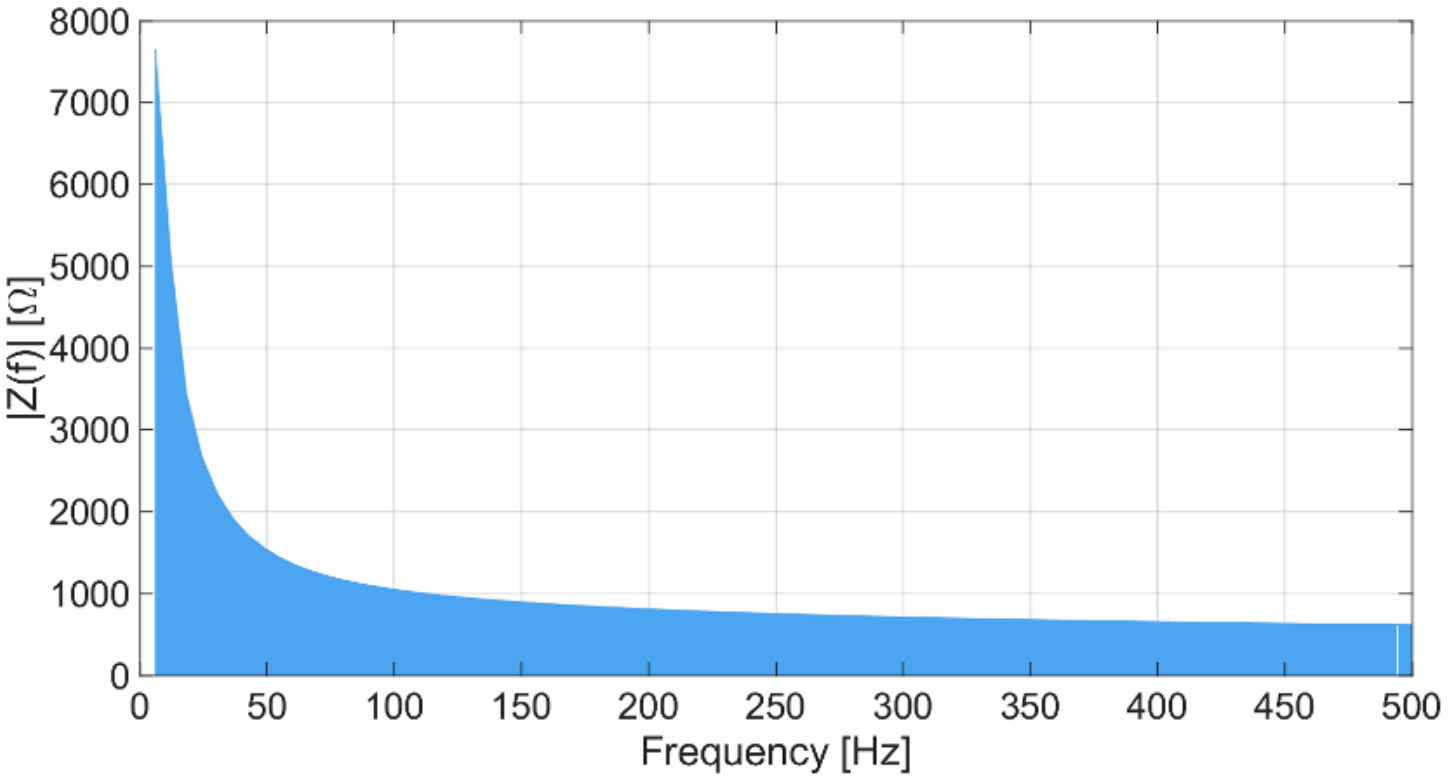


Figure 4

Absolute |*Z*| versus frequency in vivo at coherence ³0.5 (MATLAB R2024b)

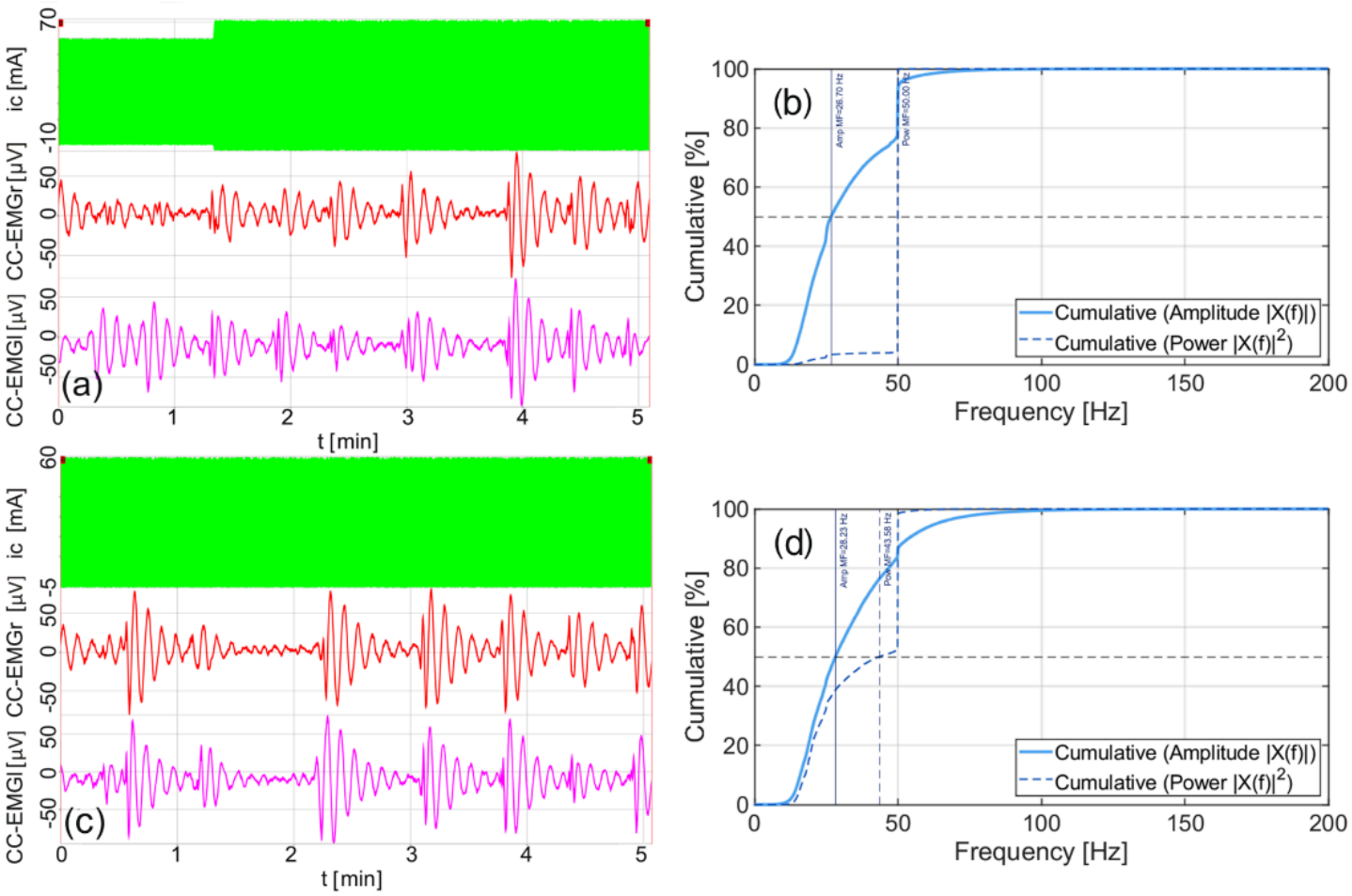


Figure 5

Records of CC-EMG in the left and right CC-EMG, and the amplitude and corresponding power spectrum cumulative curves while the left and right NVB were stimulated. (a) i_c (top trace), CC-EMGr (intermediate trace) and CC-EMGl while the left NVB was stimulated. (b) Amplitude and power spectrum cumulative curve for CC-EMGr. (c) i_c (top trace), CC-EMGr (intermediate trace) and CC-EMGl while the right NVB was stimulated. (d) Amplitude and power spectrum cumulative curve for CC-EMGl